THE ARCHIVE OF MECHANICAL ENGINEERING

Vol. XLIX 2002 Number 1

Key words: *vibrations, bifurkation, numerical simulation, vehicle suspension*

RYSZARD ANDRZEJEWSKI[*)], *JERZY WERNER*[*)]

VIBRATIONS OF THE NON-LINEAR THREE-BODY WHEELED VEHICLE MODEL. BIFUKATOINS AND CHAOTIC

The paper presents theoretical analysis of excited vibrations of the vehicle in a wide range of excitation frequencies (from 1 to 80 Hz). The mathematical model and calculations were prepared for the accepted physical model of the vehicle. The model was used to simulate the excited vertical vibrations. The bifurcation figures with an excitation frequency as a bifurcation parameter were determined on the basis of the simulation results – the changes of kinematics values in time. Bifurcation diagrams give a picture of vehicle vibrations. This picture gives the possibility of identification of characteristic parameters of sprigs and dumping elements and can be used for control, diagnostic aims, and for making technical investigations of vehicle suspension.

NOTATION

A, B – point - front or rear arm joint,

OF, OR – point - front or rear axle,
F, R – point - front or rear wheel contact plane with the road surface,
Z – vertical displacement of body mass centre,
$\ddot{z}$, $\frac{d^2z}{dt^2}$ – second derivative of the displacement z on time t,
ε – rotation angle of the vehicle body,
$\ddot{\varepsilon}$, $\frac{d^2\varepsilon}{dt^2}$ – second derivative of the angular displacement ε on time t,
z_F, z_R – vertical displacement of front or rear arm joint,
z_{OF}, z_{OR} – vertical displacement of front or rear wheel,
f_{sF}, f_{sR}. – displacement of suspension front or rear elements,
h_F, h_R – kinematics excitation (resulting for ex. road profile),

*) *Institute of Vehicle, Technical University of Lodz, ul. Stefanowskiego 1/15,90-924 Łódź, Poland; E-mail: andrr@ck-sg.p.lodz.pl*

φ_F, φ_R – front or rear wheel angle of rotation,
β_F, β_R – angular displacement of front or rear suspension spring and dumping elements,
α_F, α_R – angular displacement of front or rear suspension arm
m – body mass,
J – body inertia moment according to the mass centre,
m_F, m_R – front or rear wheel mass,
J_F, J_R – inertia moment of the front or rear wheel (according to the axis of rotation),
F_{sC}, F_{sD} – force in the spring element of the front or rear suspension,
F_{tC}, F_{tD} – force in the dumping element of the front or rear suspension,
F_{zF}, F_{zR} – vertical force acting from the road surface on the front or rear wheel,
F_{xF}, F_{xR} – horizontal force acting from the road surface on the front or rear wheel,
M_{TF}, M_{TR} – friction torque of braking element of the front or rear wheel,
R_{KF}, R_{KR} – dynamic radius of the front or rear wheel,
L_{AOF} – front suspension arm length,
L_{BOR} – rear suspension arm length.

1. Description of investigated object. Vehicle model

The object of investigations is a vehicle model with a body connected to wheels by single longitudinal arms, in the front pushed arm, in the rear – trailed arm – Fig. 1 and Fig. 2. Suspension system with longitudinal arms gives the model a general character, because the kinematics of any suspension system can be presented using the kinematics of an artificial arm with „transient" length and with a „transient" centre of rotation. The model consists of a flat system of inertia elements ((*m*, *J*), (m_F, J_F) and (m_R, J_R)), and elements without inertia ((A–OF) and (B–OR)), connected by the spring and dumping elements. It was accepted that the model of tyres is also non-linear.

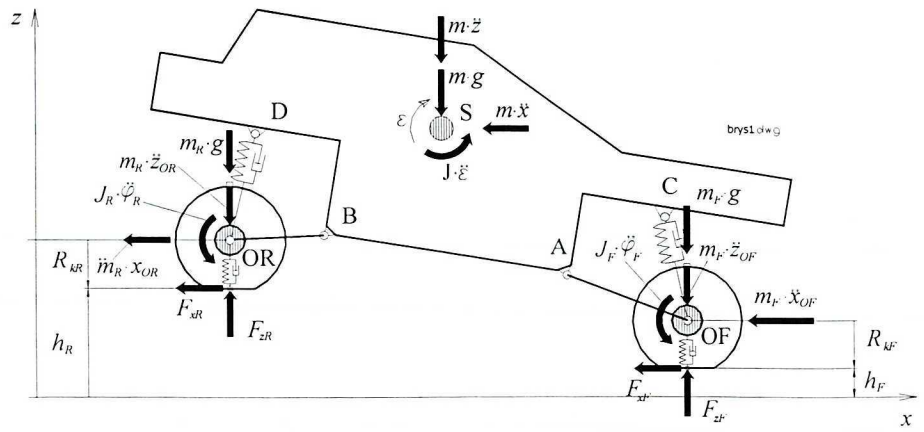

Fig. 1. Vehicle model

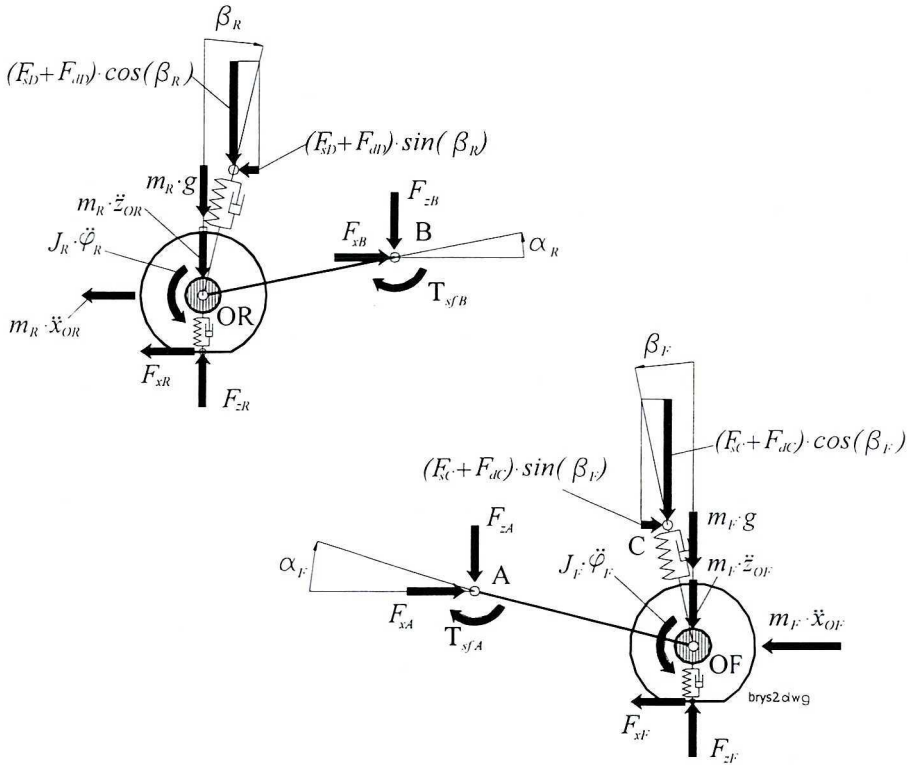

Fig. 2. Vehicle suspension model

Dumping forces in the suspension shock absorbers are described using the following equations :

$$\text{for } \frac{df_s}{dt} < 0 \qquad F_t = 0.6 \cdot C_t \cdot \left[\left(\frac{df_s}{dt} \right) + 0.1 \cdot \left(\frac{df_s}{dt} \right)^2 + 0.006 \cdot \left(\frac{df_s}{dt} \right)^3 \right],$$

$$\text{for } \frac{df_s}{dt} > 0 \qquad F_t = C_t \cdot \left[\left(\frac{df_s}{dt} \right) - 0.1 \cdot \left(\frac{df_s}{dt} \right)^2 + 0.006 \cdot \left(\frac{df_s}{dt} \right)^3 \right],$$

$$\text{for } \frac{df_s}{dt} = 0 \qquad F_t = 0,$$

where coefficient C_t for the front (F) and rear (R) axle: $C_{tF} = 2400$ [N/(m/s)] and $C_{tR} = 3500$ [N/(m/s)].

The considered vehicle model is a system with 7 degrees of freedom, as one can see in Fig. 1, 2. The generalised co-ordinates accepted here are the following kinematic values: ε, x_S, z_S, α_F, α_R, φ_F, φ_R. These values are shown with the vehicle model in Fig. 3.

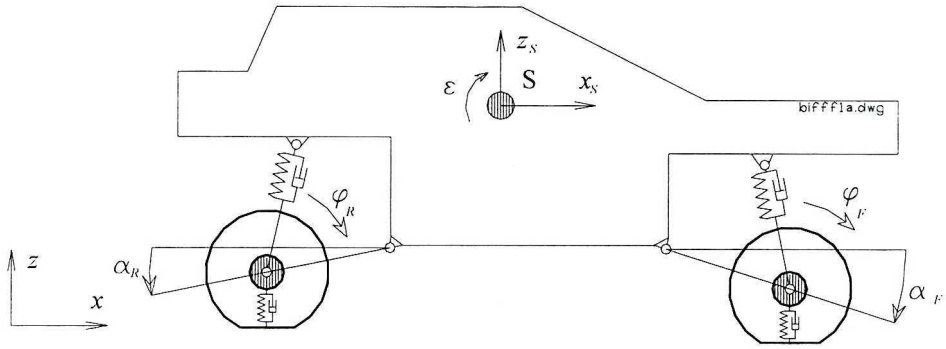

Fig. 3. Generalized co-ordinates for vehicle model ε, x_S, z_S, α_F, α_R, φ_F, φ_R

The following quantities were introduced:

$$q_1 = \frac{d\varepsilon}{dt}, \quad q_2 = \varepsilon, \quad q_3 = \frac{dx_S}{dt}, \quad q_4 = x_S, \quad q_5 = \frac{dz_S}{dt}, \quad q_6 = z_S,$$
$$q_7 = \frac{d\alpha_F}{dt}, \quad q_8 = \alpha_F, \quad q_9 = \frac{d\alpha_R}{dt}, \quad q_{10} = \alpha_R, \quad q_{11} = \frac{d\varphi_F}{dt}, q_{12} = \varphi_F,$$
$$q_{13} = \frac{d\varphi_R}{dt}, \quad q_{14} = \varphi_R.$$

Basic equations of the vehicle model motion – Fig. 1, 2, 3 – were presented as a system of derivative equations $\frac{dq_i}{dt}(q_i,...)$.

$$\frac{dq_1}{dt} = \Big\{F_{zB}\cdot(q_4 - x_B) + F_{xB}\cdot(q_6 - z_B) - \Big[F_{zA}\cdot(x_C - q_4) + F_{xA}\cdot(q_6 - z_A) +$$
$$+\big[F_{sD} + F_{tD}\big]\cdot\cos(\beta_R)\cdot(q_4 - x_D)\Big] - \Big[(F_{sD} + F_{tD})\cdot\sin(\beta_R)\cdot(q_6 - z_D) - \;;$$
$$-(F_{sC} + F_{tC})\cdot\cos(\beta_F)\cdot(x_C - q_4)\Big] + (F_{sC} + F_{tC})\cdot\sin(\beta_F)\cdot(q_6 - z_C)\Big\}\cdot\frac{1}{J}$$

$$\frac{dq_2}{dt} = q_1,$$

$$\frac{dq_3}{dt} = \frac{-F_{xR} - F_{xF}}{m + m_F + m_R},$$

$$\frac{dq_4}{dt} = q_3,$$

$$\frac{dq_5}{dt} = \Big[-m\cdot g + F_{zB} + F_{zA} + (F_{sD} + F_{tD})\cdot\cos(\beta_R) + (F_{sC} + F_{tC})\cdot\cos(\beta_F)\Big]\cdot\frac{1}{m},$$

$$\frac{dq_6}{dt} = q_5,$$

$$\frac{dq_7}{dt} = \frac{m_F \cdot g - F_{zF} + F_{zA} + (F_{sC} + F_{tC}) \cdot \cos(\beta_F)}{m_F \cdot \cos(q_8) \cdot L_{AOF}} + \frac{\frac{d^2 z_{OF}}{dt^2}}{\cos(q_8) \cdot L_{AOF}} + \frac{\sin(q_8)}{\cos(q_8)} \cdot \left(\frac{dq_8}{dt} \right)^2,$$

$$\frac{dq_8}{dt} = q_7,$$

$$\frac{dq_9}{dt} = \frac{m_R \cdot g - F_{zR} + F_{zB} + (F_{sD} + F_{tD}) \cdot \cos(\beta_R)}{m_R \cdot \cos(q_{10}) \cdot L_{BOR}} + \frac{\frac{d^2 z_{OR}}{dt^2}}{\cos(q_{10}) \cdot L_{BOR}} + \frac{\sin(q_{10})}{\cos(q_{10})} \cdot \left(\frac{dq_{10}}{dt} \right)^2,$$

$$\frac{dq_{10}}{dt} = q_9,$$

$$\frac{dq_{11}}{dt} = -\frac{M_{TF}}{J_{KF}} + \frac{F_{xF} \cdot R_{KF}}{J_{KF}},$$

$$\frac{dq_{12}}{dt} = q_{11},$$

$$\frac{dq_{13}}{dt} = -\frac{M_{TR}}{J_{KR}} + \frac{F_{xR} \cdot R_{KR}}{J_{KR}},$$

$$\frac{dq_{14}}{dt} = q_{13}.$$

The derivative equations system $\frac{dq_i}{dt}(q_i,...)$ was solved using the numerical procedure Runge-Kutta IV. The time step for calculation was constant at the level of $\Delta t = 2^{-12}$ [s], it means: $\Delta t = 0.000244140625$ [s]. The step value was chosen after many tests and numerical investigations.

2. Simulation tests

Simulation numerical tests were developed using this system model and vehicle model. Excitation of vibrations was done in two cases :

- excitation for front wheels $h_F(t) = a_{har} \cdot \sin(2 \cdot \pi \cdot n \cdot t)$,
- excitation for front and rear wheels simultaneously:

$h_F(t) = a_{har} \cdot \sin(2 \cdot \pi \cdot n \cdot t)$ and $h_R(t) = a_{har} \cdot \sin(2 \cdot \pi \cdot n \cdot t)$.

Simulations were performed for different values of excitation frequencies from $n = 1$ to $n = 80$ [Hz]. Amplitude of excitation had constant value for all simulations at the rate of $a_{har} = 0.02$ [m].

Initial values for simulation

From one point of view, the vehicle body behaviour (motion, vibrations) might be interesting, from the other – behaviour of wheels (motion, displacement) is

interesting when one investigates vehicle vertical vibrations. The first problems are important when one pays attention to travelling comfort, the second – when safety of travel is considered. The following initial values were accepted for these reasons :

z_A, z_B [m] – body vertical displacement for point A, B – Fig.1,

$\frac{dz_A}{dt}$, $\frac{dz_R}{dt}$ [m/s] – velocity of body vertical displacement for point A, R,

z_{OF}, z_{OR} [m] – wheel vertical displacement for point OF, OR,

$\frac{dz_{OF}}{dt}$, $\frac{dz_{OR}}{dt}$ [m/s] – velocity of wheel vertical displacement for point OF, OR.

Vehicle parameters

The values of basic parameters for the investigated vehicle model were accepted as follows:

vehicle body mass – $m = 1400\,[\mathrm{kg}]$,

body inertia moment according to the centre of mass – $J = 1200\,[\mathrm{kg \cdot m^2}]$,

mass of the front or rear wheel with suspension elements – $m_F = 30\,[\mathrm{kg}]$, $m_R = 25\,[\mathrm{kg}]$,

wheel inertia moment (according to the wheel axle) for front or rear wheel – $J_F = 2\,[\mathrm{kg \cdot m^2}]$, $J_R = 1.5\,[\mathrm{kg \cdot m^2}]$,

stiffness coefficient for front or rear suspension – $K_{sF} = 25000\,[\mathrm{N/m}]$, $K_{sR} = 20000\,[\mathrm{N/m}]$,

dumping coefficient for front or rear suspension – $C_{tF} = 2400\,[\mathrm{N/(m/s)}]$, $C_{tR} = 3500\,[\mathrm{N/(m/s)}]$,

suspension arm length for front or rear – $L_{AOF} = 0.5\,[\mathrm{m}]$, $L_{BOR} = 0.5\,[\mathrm{m}]$,

wheel free radius – $R_{KFsw} = 0.25\,[\mathrm{m}]$, $R_{KRsw} = 0.25\,[\mathrm{m}]$.

Other parameters (length and other dimensions of the vehicle model) are similar to those of European passenger car of lower middle class.

3. Simulation tests results

Series of initial values were received as the result of computer simulation done for the investigated system model. They were the basis for plotting the bifurcation diagrams, according to the procedure described in Supplement 1. The excitation frequency – n [Hz] was accepted as the bifurcation parameter.

The series of bifurcation curve values were created for sampling time delay $t_0 = 0$:

$$\left\{ z_i(t)\Big|_{t=t_0+n\cdot k}, n \right\} \quad \text{and} \quad \left\{ \frac{dz}{dt_i}(t)\Big|_{t=t_0+n\cdot k}, n \right\}$$

The results were recorded after receiving a steady state of vibrations in order to avoid the influence of initial transient state in the system.

3.1. Excitation acting on front wheels

The bifurcation diagrams $\left\{\frac{dz_A}{dt}, n\right\}$, and $\{z_{OF}, n\}$ are shown in Fig. 4, where $\frac{dz_A}{dt}$ – vertical displacement velocity for vehicle body point A, z_{OF} – vertical displacement for front wheel point OF. The curves were drawn for standard parameter values for vehicle suspension model: $C_{tF} = 2400\,[\mathrm{N/(m/s)}]$. System vibrations – (for vehicle model) have a harmonic character. The characteristic feature of the presented curves is the following phenomenon: bifurcation branch appears at excitation frequency of approx. 35 [Hz]. This bifurcation disappears at a frequency of approx. 78 [Hz].

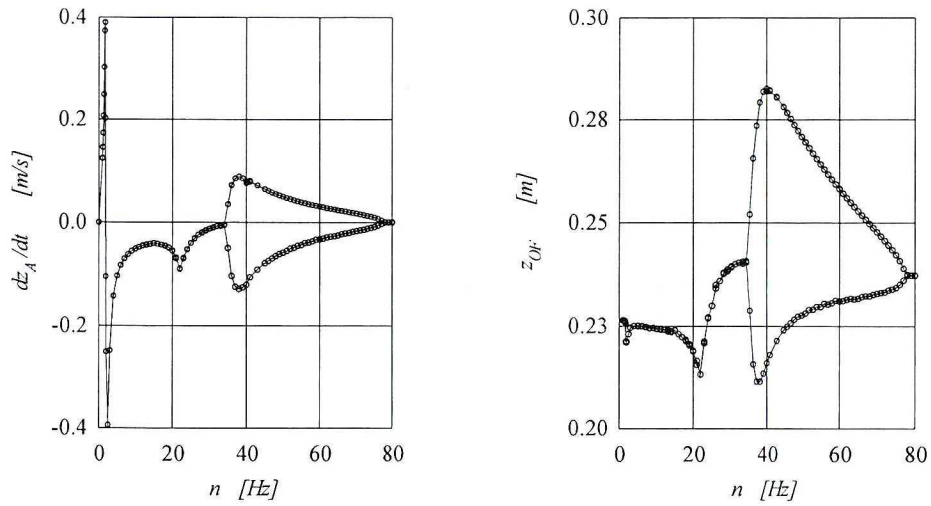

Fig. 4. Bifurcation diagrams showing body vibrations for point A $\left\{\frac{dz_A}{dt}, n\right\}$ and showing front wheel vibrations – $\{z_{OF}, n\}$. Dumping coefficient for front suspension standard value – C_{tF} =2400 [N/(m/s)]. Excitation on front axle

The bifurcation diagrams $\left\{\frac{dz_A}{dt}, n\right\}$ and $\{z_{OF}, n\}$ are shown in Fig. 5, for lower value of parameter describing damping of the front suspension shock absorber $C_{tF} = 1800\,[\mathrm{N/(m/s)}]$, it means for a lower dumping of vibration. The system vibrations are of harmonic character, for majority of vibrations frequency values. The characteristic feature of the curves is that, similarly as in Fig. 4, the

bifurcation appears here in the range of excitation frequencies approx. 34÷78 [Hz]. The secondary branch – bi-bifurcation appears in the range of excitation frequencies of approx. 54÷65 [Hz], for curves $\left\{\frac{dz_A}{dt}, n\right\}$ and $\{z_{OF}, n\}$.

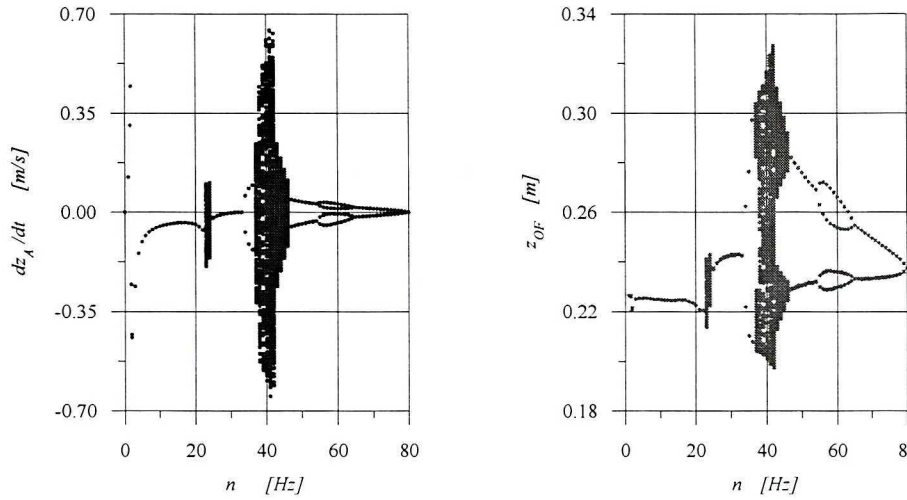

Dumping coefficient - CtF = 1800 [N/(m/s)]

Fig. 5. Bifurcation diagrams showing body vibrations for point A – $\left\{\frac{dz_A}{dt}, n\right\}$ and showing front wheel vibrations – $\{z_{OF}, n\}$. Dumping coefficient for front suspension lower value – C_{tF} =1800 [N/(m/s)]. Excitation on front axle

The characteristic values of bifurcation diagrams are given in Table 1. These are: the range of excitation frequencies for bifurcation, bifurcation amplitude and the range of excitation frequencies for bi-bifurcation appearance.

Table 1.

The characteristic values of bifurcation curves

Bifurcation diagrams /vehicle data	The range of bifurcation appearance n [Hz]	Amplitude (dual) of bifurcation	The range of bi-bifurcation appearance n [Hz]
$\left\{\frac{dz_{OF}}{dt}, n\right\}$ / standard data	35 ÷ 78	0.22 [m/s]	–
$\{z_{OF}, n\}$ / standard data	35 ÷78	0.071 [m]	–
$\left\{\frac{dz_{OF}}{dt}, n\right\}$ / $C_{tF} \langle C_{tF\ std}$	32 ÷76	1.3* [m/s]	54÷65
$\{z_{OF}, n\}$ / $C_{tF} \langle C_{tF\ std}$	32 ÷76	0.13** [m]	54÷65

*, ** – amplitude values are not for curves with bifurcation, but for chaotic vibrations with maximal amplitude

The Poincare maps were additionally presented in Fig. 6, 7 and 8 for a better explanation of bifurcation curves for vehicle model with lower front suspension dumping – Fig. 5. These curves were drawn for such excitation frequencies at which the non-harmonic motion was presented in bifurcation curves.

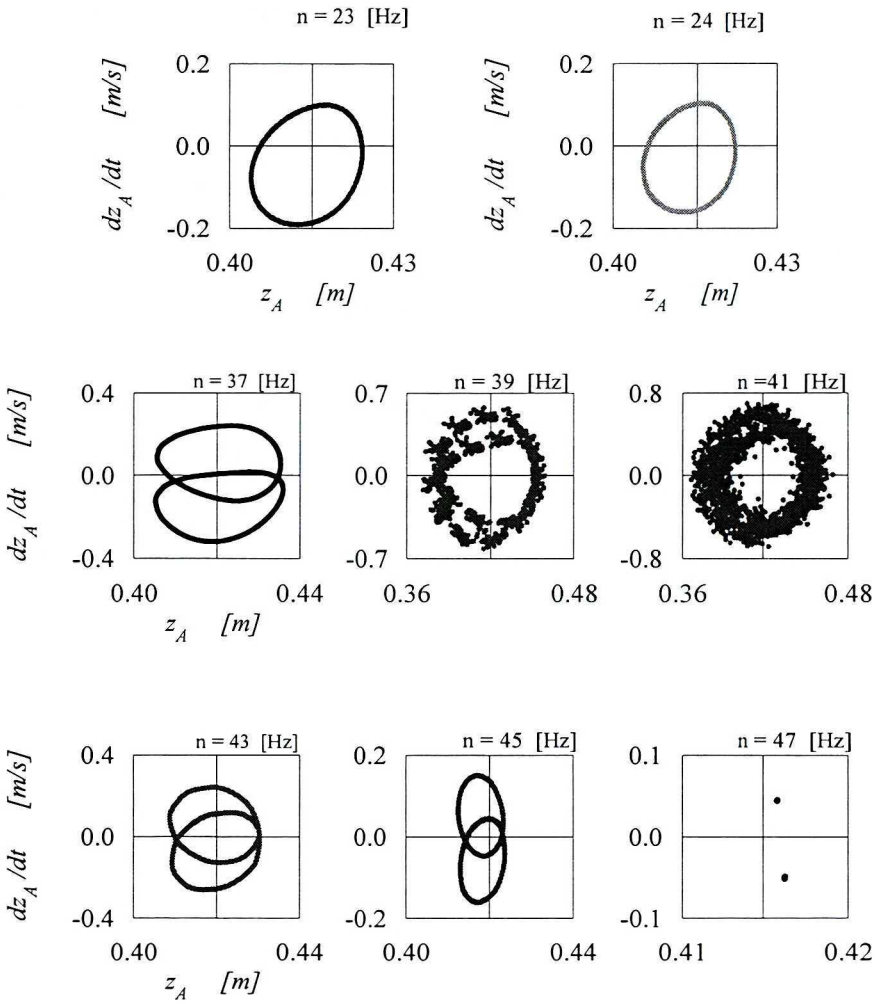

Fig. 6. Poincare maps showing body vibrations for point A $\left\{\frac{dz_A}{dt}, z_A\right\}$. Dumping coefficient for front suspension lower value – C_{tF} =1800 [N/(m/s)]. Excitation on front axle for selected excitation frequencies

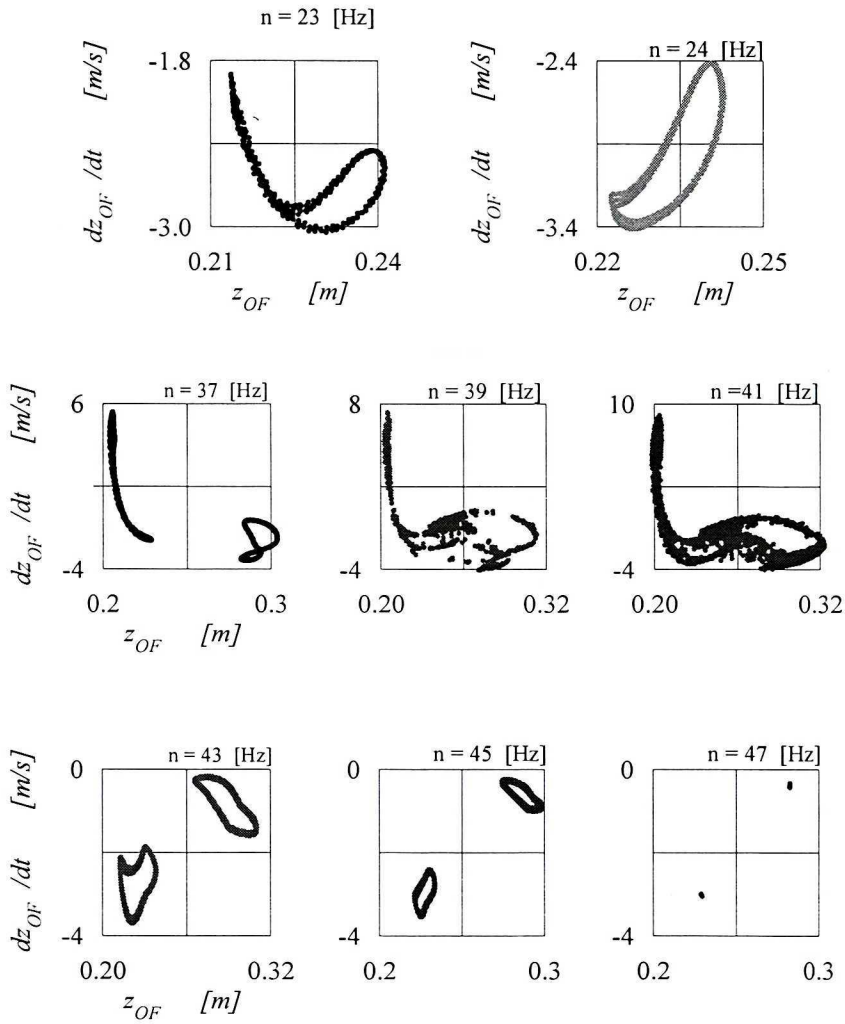

Fig. 7. Poincare maps showing front wheel vibrations $\left\{\frac{dz_{OF}}{dt}, z_{OF}\right\}$, Dumping coefficient for front suspension lower value – C_{tF} =1800 [N/(m/s)]. Excitation on front axle for selected excitation frequencies

Analysing the bifurcation diagrams – Fig. 5 – and Poincare map – Fig. 6 – one can see that point A (mounting point for front arm) vertical motion has a character of quasi harmonic motion with dual loop curves for $\frac{dz_A}{dt}(z_A)$. For the excitation frequency 37 [Hz], point A vertical motion has also a quasi-harmonic character with dual loop curves $\frac{dz_A}{dt}(z_A)$, but the amplitude of this motion is severed times higher than the previous one. At excitation frequency of 39 [Hz],

point A vertical motion has also quasi harmonic character with dual loop curves $\frac{dz_A}{dt}(z_A)$, but one can observe some chaotic behaviour. At excitation frequency 41 [Hz], point A vertical motion has also chaotic character. For higher values of excitation frequency – for $n = 43$ and $n = 45$ [Hz] – system motion comes back to quasi harmonic motion with dual loop curves $\frac{dz_A}{dt}(z_A)$, and at excitation frequency $n = 47$ [Hz] one can see harmonic motion with bifurcation.

Poincare maps are shown in Fig. 7 $\frac{dz_{OF}}{dt}(z_{OF})$ – describing point OF motion (front wheel vertical motion). These maps concern bifurcation curves $z_{OF}(n)$, which were drawn for lower dumping ($C_{tF} = 1800$ [N/(m/s)] – Fig. 5.

Basing on bifurcation diagrams – Fig. 5 – and Poincare map – Fig. 7 – one can see that at excitation frequencies 23 and 24 [Hz] front wheel point OF vertical motion is a quasi harmonic motion. At excitation frequency 37 [Hz], point OF vertical motion has quasi harmonic character with dual loop curves $\frac{dz_{OF}}{dt}(z_{OF})$. At excitation frequency 39 [Hz] point OF motion maintains the character of quasi harmonic motion with dual loop curves $\frac{dz_{OF}}{dt}(z_{OF})$, but there are some symptoms of chaotic motion. For the following values of excitation frequencies – $n = 43$ and $n = 45$ [Hz] – the system motion is quasi harmonic with dual loop curves, but at excitation frequency $n = 47$ [Hz] one can see harmonic motion with bifurcation.

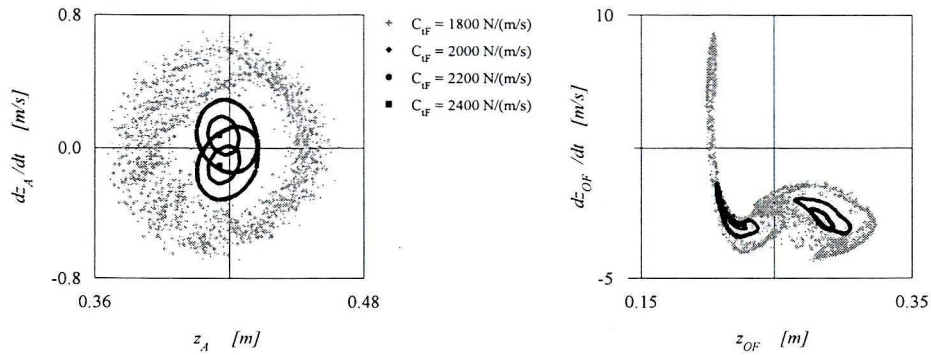

Fig. 8. Poincare maps showing body vibrations for point A – $\left\{\frac{dz_A}{dt}, z_A\right\}$ and showing front wheel vibrations $\left\{\frac{dz_{OF}}{dt}, z_{OF}\right\}$ for different values of front suspension dumping coefficient Ct_F. Excitation on front axle at frequency 41 [Hz]

Poincare map $\frac{dz_A}{dt}(z_A)$ is presented in Fig. 8 for excitation frequency 41 [Hz]. The influence of dumping on system motion is shown in this figure. As it results from the presented map, and also from Fig. 6, for dumping coefficient $C_{tF} = 1800\,[\mathrm{N/(m/s)}]$ point A motion (body motion) has a chaotic character. The increase of dumping (for this kind of excitation) causes a change in vibration character – for $C_{tF} = 20000\,[\mathrm{N/(m/s)}]$ motion stops to be chaotic and it evolves quasi harmonic with two loops. Further increase of dumping coefficient value results in amplitude decrease $\frac{dz_A}{dt}$ and z_A, and for $C_{tF} = 2400\,[\mathrm{N/(m/s)}]$ the motion becomes harmonic with bifurcation.

3.2. Excitation acting simultaneously on front and rear wheels.

The kinematic input signals on front wheels and rear wheels are described by following equstions:

$$h_F(t) = a_{har} \cdot \sin(\omega \cdot t) \quad \text{and} \quad h_R(t) = a_{har} \cdot \sin(\omega \cdot t)\,.$$

Some results of investigations obtained for standard values of suspension parameters and for excitation acting simultaneously on front and rear wheels are presented in Fig. 9.

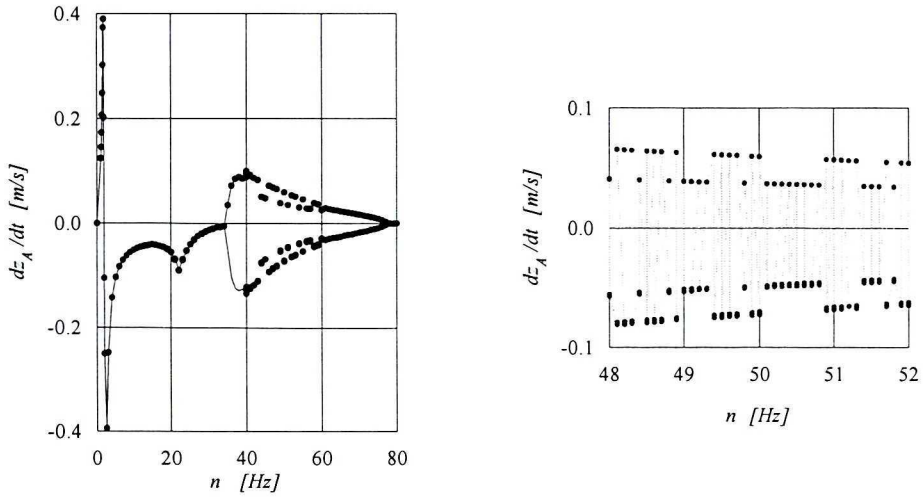

Dumping coefficient - CtF = 2400 [N/(m/s)]

Fig. 9. Bifurcation diagrams showing body vibrations for point A – $\left\{\frac{dz_A}{dt}, n\right\}$. Dumping coefficient for front suspension standard value – C_{tF} =2400 [N/(m/s)]. Excitation on front and rear axles – simultaneously

For the case of vibration excitation acting simultaneously on front and rear wheels, bifurcation diagrams have a different shape than that for vibration excitation acting on one wheel axle – see Fig. 4. In Fig. 9 one can see bifurcation and also pulsation impulse change of the value $\frac{dz_A}{dt}$. Character of this pulsation is shown exactly at frequency range $n = 48 \div 52\,[\mathrm{Hz}]$.

4. Conclusions

In this paper, the authors present the results of simulation tests for vehicle model whose structure is shown in Fig. 1, 2, also with non-linear characteristics of spring and dumping elements. The assumed values of parameters and inertia elements for this vehicle model were similar to those of passenger car of European lower middle class. The excitation for vehicle model was harmonic. The excitation character was the same as that acting on a vehicle running on a road of certain profile or during investigation on seismic test bed. The tests were carried out for two cases:

1. excitation acting on vehicle front wheels,
2. excitation acting on vehicle front and rear wheels simultaneously.

The results of these tests are presented as bifurcation diagrams and Poincare maps – Figs. from 4 to 9.

The following conclusions were drawn on the basis of the analysis of bifurcation diagrams:

- In the case of excitation acting on the wheels of one axle, bifurcation diagrams $\left\{\frac{dz_A}{dt}, n\right\}$, $\{z_{OF}, n\}$ the curves are **smooth (continuous)** – Fig. 4.
- Bifurcation has the shape of **snake head** – Fig. 4. This bifurcation appears in the range of 34 to 80 Hz.

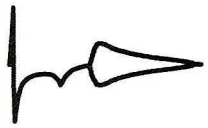

- In the case of lower, insufficient suspension dumping, one can see dual loop in bifurcation diagrams – bi-bifurcation – Fig. 5. Bifurcation has the shape of **snake head with glasses**.

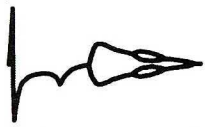

- In the case of lower, insufficient suspension dumping, in some range of excitation frequency, some symptoms of quasi harmonic motion can be observed – see bifurcation diagrams in Fig. 5 and Poincare maps in Fig. 6, 7 and 8.

- In the case of lower, insufficient suspension dumping, in some range of excitation frequencies, some symptoms of chaotic motion can be observed – see bifurcation diagrams in Fig. 5 and Poincare maps in Fig. 6, 7 and 8.

- In the case of excitation acting simultaneously on front and rear wheels, **pulse slit** can be observed in bifurcation diagrams, values pulsation showing instability of function – $\left\{\frac{dz_A}{dt}, n\right\}$ – Fig. 9.

- Bifurcation diagrams created for excitation frequencies ranging from 1 to 80 Hz are the picture of vehicle model vibration, which can be changed by introducing changes in the parameters of vehicle suspension characteristic.
- Changes (approx. 25%) of parameters values for the tests results presented here, connected with dumping, had a serious influence on the shape of bifurcation diagrams, both in quantitative and in qualitative sense.
- **The sensivity** of shape of bifurcation diagrams with respect to the changes of values of parameters characteristics of vehicle suspension damping is so high that the bifurcation diagram can be used for **identification** of these characteristics or for estimation of suspension technical state.

***

APPENDIX

The method of deriving bifurcation diagrams.
Bifurcation curves are the picture of vibrations of a system, whose motion is excited by harmonic pulses. One can obtain bifurcation curves by making initially the so called Poincare maps.

Poincare map

One can describe model vibrations with the system of derivative equations

$$\frac{dz_i}{dt} = f\left(z_i, t, h(n,t)\right),$$

where $h(n, t)$ is harmonic excitation with frequency n, so Poincare map is a class

$$\left\{ z_i(t), \frac{dz_i}{dt}(t)\Big|_{t=t_0+n\cdot k,\ k=1,2,3,\ldots} \right\},$$

where t_0 – sampling time delay versus time moment describing the excitation wave begining.

Bifurcation diagrams

One can describe the so called bifurcation parameter (i.e. frequency, excitation amplitude,...) – PB. Then, one can prepare some classes – Poincare maps – for next values of bifurcation parameter – PB. Making projection on axis z_i or $\frac{dz_i}{dt}$ for following Poincare maps one can have classes

$$\left\{ z_i(t)\Big|_{t=t_0+n\cdot k}, PB \right\} \quad \text{or (and)} \quad \left\{ \frac{dz_i}{dt}(t)\Big|_{t=t_0+n\cdot k}, PB \right\}$$

Bifurcation diagrams are graphic representation of the above mentioned classes.

Manuscript received by Editorial Board, November 19, 2001;
final version, March 11, 2002.

REFERENCES

[1] Awrejcewicz J.: Bifurcation and chaos. Theory and Application. Springer-Verlag, Berlin, Heideberg, New York, 1994.

[2] Kapitaniak T.: Chaotic oscillations in mechanical systems. Manchester University Press, Manchester 1991.

[3] Andrzejewski R.: Stabilność ruchu pojazdów kołowych. WNT Warszawa 1997.

[4] Michelberger P., Palkovics L., Stepan G.: Chaotic behaviour of the non-linear wheel suspension. Machine Vibration (1993) 2, pp. 47÷53.

[5] Weispfenning Th.: Fault detection and diagnosis of components of the vehicle vertical dynamics. 1st International Conference on Control and Diagnostics in Automotiv Applications, Genova, Italy, 3–4 Oktober 1996.

Drgania nieliniowego trójmasowego modelu pojazdu kołowego. Bifurkacje i chaos

Streszczenie

W pracy opisano rezultaty symulacyjnych numerycznych badań drgań pionowych trójmasowego modelu pojazdu kołowego. Przyjęto nielinowe charakterystyki elementów sprężynujących i tłumiących zawieszania i ogumienia. Model pojazdu posadowiony był na modelach plyt sejsmicznych o pionowych harmonicznych wymuszeniach. Badania przeprowadzono dla częstości wymuszeń od 1 do 80 Hz. Wyniki badań przedstawiono w postaci wykresów bifurkacyjnych i map Poincare. Wyniki badań mogą być przydatne do prac nad systemami diagnostycznymi przeznaczonymi dla pojazdów kołowych.